Journal of Colloid and Interface Science 642 (2023) 747–756

Contents lists available at ScienceDirect

Journal of Colloid and Interface Science

journal homepage: www.elsevier.com/locate/jcis

Exploring carbonate rock wettability across scales: Role of (bio)minerals

Alicia Moya [a,b,*], Fabienne Giraud [a], Valerie Molinier [c], Yves Perrette [d], Laurent Charlet [a], Alexander Van Driessche [a,e], Alejandro Fernandez-Martinez [a]

[a] Univ. Grenoble Alpes, Univ. Savoie Mont Blanc, CNRS, IRD, IFSTTAR, ISTerre 1381 Rue de la Piscine, 38610 Gières, France
[b] Department of Inorganic Chemistry, Universidad Autónoma de Madrid Calle Francisco Tomás y Valiente 7, 28049 Madrid, Spain
[c] TotalEnergies, Pôle Etudes et Recherche de Lacq, RN117, 64170 Lacq, France
[d] CNRS, Univ. Savoie Mont Blanc, EDYTEM, 5 Bd de la Mer Caspienne, 73370 Le Bourget du Lac, France
[e] InstitutoAndaluz de Ciencias de la Tierra (IACT), CSIC – Universidad de Granada, Av. De las Palmeras 4, 18100 Armilla, Spain

GRAPHICAL ABSTRACT

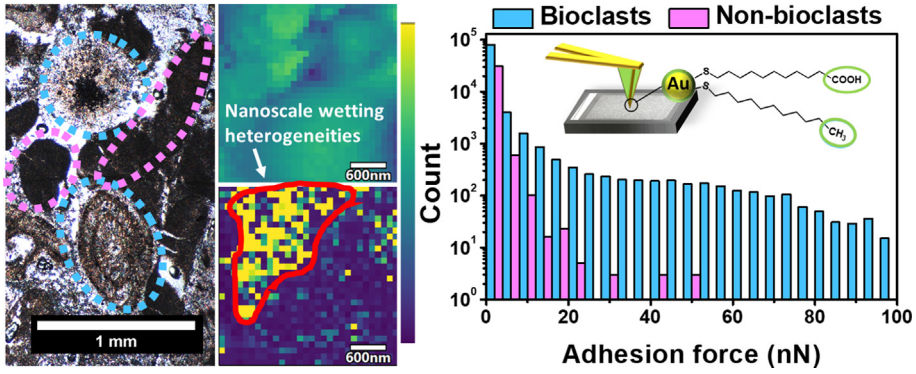

ARTICLE INFO

Article history:
Received 26 November 2022
Revised 22 March 2023
Accepted 29 March 2023
Available online 5 April 2023

Keywords:
Wettability
Carbonates
Biominerals
Adhesion force
AFM/AFS

ABSTRACT

Hypothesis: The wettability of carbonate rocks is expected to be affected by the organic components of biominerals which are complex, nanostructured organo-mineral assemblages. Elucidating the nanoscale mechanisms driving the wettability of solid surfaces will enable a better understanding of the role of biominerals in the wetting properties of carbonate rocks to control various geological, environmental and industrial processes.
Experiments: Using Atomic Force Microscopy and Spectroscopy (AFM/AFS) we probed the wettability properties of carbonate rocks with different amounts of organic material. The adhesion properties of two types of limestones were determined in liquid environments at different length scales (nm to mm) using functionalized tips with different chemical groups to determine the extent of surface hydrophobic and hydrophilic organo-mineral interactions.
Findings: We observed homogeneous hydrophobic areas at length scales below < 5 μm. The origin of this hydrophobicity is linked to the presence of organics, whose amount and spatial distribution depend on

* Corresponding author at: 1381 Rue de la Piscine, 38610 Gières, France.
E-mail addresses: alicia.moya-cuenca@univ-grenoble-alpes.fr (A. Moya), fabienne.giraud-guillot@univ-grenoble-alpes.fr (F. Giraud), valerie.molinier@totalenergies.com (V. Molinier), yves.perrette@univ-smb.fr (Y. Perrette), laurent.charlet@univ-grenoble-alpes.fr (L. Charlet), alexander.van-driessche@univ-grenoble-alpes.fr (A. Van Driessche), alex.fernandez-martinez@univ-grenoble-alpes.fr (A. Fernandez-Martinez).

https://doi.org/10.1016/j.jcis.2023.03.197

the rock composition. Specifically, our results reveal that the biogenic vs non-biogenic origin of the mineral grains is the main rock property controlling the wettability of the solid surface. Overall, our methodology offers a multi-scale approach to unravel the role that organic moieties and biominerals play in controlling the wettability of rock-water interfaces.

1. Introduction

Wettability is one of the key properties controlling fundamental physicochemical interfacial processes in fields such as the environmental sciences, geology, biology, material science and civil engineering. This includes the fluid transport of organic pollutants in the subsurface [1], radwaste geological storage [2], nucleation and growth of biominerals [3], uptakes of nutrients by plant roots [4], development of novel filtration systems with high physical stability[5], geological CO_2 sequestration [6,7], enhanced oil recovery [8], proton exchange membrane in fuel cells [9], water desalination systems [10,11], or conversion of CO_2 in the cement and concrete industry [12].

The term wettability describes the preference of a solid surface to be in contact with one type of liquid rather than another one, which is essentially determined by intermolecular attractive interactions (adhesion forces) [13]. Although wettability is very often reduced to hydrophilic (water-wet) and hydrophobic (oil-wet) behaviors [14], this simplification is masking the complexity present at real surfaces, especially when investigating heterogeneous systems such as natural rocks. Most commonly, rock wettability is determined macroscopically using contact angle measurements [15–20]. However, the question arises if this type of measurement is representative of the wettability of complex systems where the surface heterogeneities are smaller than the droplet size (~0.05 mL) that is deposited on the rock surface. Probing molecular interactions at the rock-water interface could shed light on this matter, providing not only fundamental insights on the influence that such heterogeneities have on the rock wettability at the nanoscale but also the physical and chemical mechanisms behind the complex concept of surface wettability.

Surface imaging and molecular interactions can be determined in liquid media with Atomic Force Microscopy (AFM) and Spectroscopy (AFS). In AFS, an array of force-distance measurements between the AFM tip and the sample surface are recorded, from which adhesion forces can be extracted (Fig. 1). In addition, the functionalization of the AFM tips with organic moieties allows to discern mechanistic insights into the interactions between specific organic functionalities and the scanned surfaces [21–23]. This approach has led to significant progress in the exploration of rock wettability at the atomic scale during the last few years [24–28]. For example, various AFS studies on minerals have demonstrated the different wetting behavior induced by adsorbed or dissolved ions (e.g. Mg^{2+} or SO_4^{2-}) or the presence of adsorbed organic matter [29–35]. Nevertheless, little attention has been paid to understanding the physical and chemical properties of the natural rock components, which will ultimately control the wettability in natural environments.

Ubiquitous presence in the nature of carbonate rocks and their abundant industrial uses have resulted in extensive research on understanding its wettability [36–38]. However, carbonate rocks are highly heterogeneous in terms of surface roughness, porosity and chemical composition [39,40], and despite many years of study, there is still not a general description of their wetting behavior. Importantly, carbonate rocks are usually formed through sedimentation processes, via the accumulation and lithification of fragments of micro-organism remains, which results in a large variety of structures, compositions – potentially including organic matter – and textures made of fossilized biominerals [41]. Biominerals are natural nanocomposite materials, composed of a hierarchical organization of organic molecules and a mineral matrix. This organization leads to the inherent heterogeneity of carbonate rocks down to the nanoscale [42–44]. Elucidating the role of the organic–inorganic nanostructures of the biominerals is paramount to understand the wettability of the rock surfaces, a task up to now never studied.

Here, we present a detailed investigation of molecular interactions at the carbonate rock-water interface using AFM/AFS (Fig. 1A). We have simultaneously measured topography and adhesion force maps (Fig. 1B) of the carbonate rock surfaces where each pixel corresponds to a single force-distance curve (Fig. 1C). From these curves, we determine the intermolecular – attractive or repulsive – forces between the sample and the tip either during the approach (position 1 in Fig. 1C) or retract step of the tip (position 2 in Fig. 1C). To measure hydrophobic/hydrophilic forces at the molecular level, that is, to evaluate the solid wettability properties, we used AFM tips coated with a monolayer of alkyl chains with non-polar (—CH_3, Fig. 1D) and polar (—COOH, Fig. 1E) end functional groups, that is, hydrophobic and hydrophilic nature, respectively. We performed this study from the microscale to the nanoscale and evaluated the relevant spatial scale where areas with heterogeneous surface wettability can be observed.

The samples under study are two limestone rocks, one from southern France – a non-reservoir rock (Fig. 1F) – and one from the Guinea gulf – an oil reservoir rock (Fig. 1G). The non-reservoir rock is a limestone sample with a rudstone-packstone texture (10 % of grains greater than 2 mm), with different types of porosity, and mainly composed of bioclast-type grains (echinoderms, bryozoans, red algae, mollusks, small benthic foraminifera). The reservoir rock is a limestone sample with a grainstone-packstone texture (grains < 2 mm), with different types of porosity, and is mainly composed of peloid-type grains and a few bioclast-type grains (echinoderms, mollusks). The use of these two contrasting rocks with significant differences in the bioclastic abundance (Fig. 1H) as well as in the adsorbed organic matter (potentially higher in the oil reservoir rock), allows to determine the effect on wetting properties of foreign organic matter over the organic remains inherent from the bioclasts. Importantly, our observations at the nanoscale are carefully performed in selected regions previously identified from optical microscopy and classified as bioclast (fragments from identified biomineral remains) vs non-bioclast (fragments unrecognized as having a direct biomineral origin, likely peloids or intraclasts from diagenetic recrystallization) grains. This approach allows unraveling the role of organic matter and the role of biominerals in the wettability of carbonate rocks.

2. Materials and methods

2.1. Materials

Blocs of limestone samples were provided by TotalEnergies collected from South East France (a non-reservoir limestone) and central Africa (a reservoir limestone). The non-reservoir limestone was

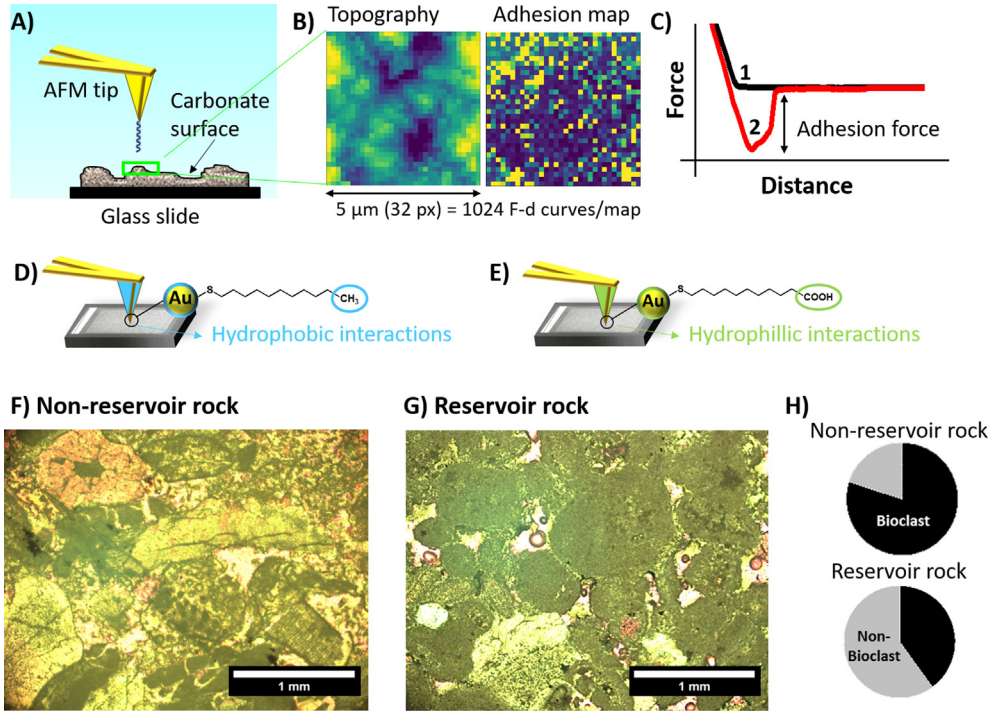

Fig. 1. (A) Schematic representation of the functionalization strategy used in this work by using AFM tips to measure intermolecular forces (adhesion forces) at the rock-water interface. We used non-polished thin sections of the carbonate rocks and performed AFS experiments where (B) topographical and adhesion force maps are obtained. Each pixel of those maps corresponds to force-distance curves as the one represented in (C). We used AFM tip coated with alkyl chains with (D) methyl (—CH_3) and (E) carboxyl acid (—COOH) end groups to study hydrophobic and hydrophilic interactions, respectively. (F) Optical image of the non-reservoir and (G) reservoir rock taken using plane-polarized light (PPL) and H) pie chart containing the percentage of bioclasts (in black) for each rock which shows a higher content of bioclasts in the non-reservoir rock which are quite well-preserved.

formed during the Upper Tertiary period, Miocene epoch, Burdigalian stage. It comprises mostly calcite (see Tables S1 and S2). This limestone is a bioclastic carbonate rock with a dual porosity system with macro and micropores (inter- and intragranular) and dual pore throats distribution with a maximum of ~6.8 and ~0.2 µm. Its specific area is ~0.46 m^2/g, the total porosity is around 32 % and permeability is ~100–300 mD. The reservoir limestone is a medium to coarse oncoidal-bioclastic grainstone of mostly calcite (see Tables S1 and S2) with dual porosity (inter- and intragranular porosity) and dual pore throats distribution with a maximum at ~10 and ~0.1 µm. Its total porosity is around 20 % and permeability is ~100–200 mD. The core of both limestones was washed with toluene and isopropanol before their use to avoid any possible organic contaminant. Then, the cores were dried at 80 °C and stored dry. Thin sections (40 µm thick) were prepared by cutting the core longitudinally and/or transversely and used indistinctly for all the experiments shown in this work. These sections were non-covered and non-polished to modify as little as possible the topographical and surface features of the different components of the carbonate rocks. The resulting thin sections were safely stored to avoid contamination. Prior each measurement, the thin sections were cleaned with ethanol and dried with N_2 to avoid contamination from the adsorption of organic matter. Thus, the non-reservoir rock should predominantly contain organic matter intrinsic to the biogenic constituents of the rock, whereas reservoir rocks could also contain homogeneously distributed oil residues. In all our thin sections, all the minerals were cut showing a new surface that mimics natural processes where new surfaces appear as a consequence of dissolution and precipitation processes. This allowed to access to organic matter trapped in the mineral structure as a consequence of the biomineralization processes (non-reservoir rock case) and evaluate the effect on the wettability of oil adsorbed through the pores (reservoir rock case).

2.2. Characterization of materials

A polarizing light microscope (Olympus) was employed at 5-10X magnification for petrographic observations and paleontological identification of the constituents of the carbonate rock. Electron microscopy images of carbonate thin sections have been acquired using a Vega3 Tescan Scanning Electron Microscope (SEM). Phase analysis was performed using X-ray Diffraction (XRD), Bruker D 8 Advance v1 on the carbonate thin sections using Cu Kα radiation. ICP-AES analysis were performed after dilution x100.000 in a Varian 720ES, detection range 0.05–50 ppm. Calibration with CMS multielement standards doped in Ca were used to be close to calcite matrix and being more accurate. Raman spectra were obtained with a LabRAM Soleil Horiba Raman microspectrometer with 532 nm wavelength laser-excitation and 1 µm spot size. Peaks were fitted using mixed Lorentzian functions using Quasar software [45]. A laser power of 15 mW was used, which we confirmed to be sufficiently low to avoid damage in the sample by the laser. Fluorescence spectra were obtained with an experimental device for stationery and time-resolved fluorescence. Both fluorescence spectra were acquired by a nanosecond pulsed YAG laser beam excitation (266 and 355 nm, 1 µJ). The sample was set on a two axes translation stage to achieve fluorescence maps. With a confocal optical set-up, the 15 µm focused beam excited the sample orthogonally and the fluorescence scattering is analyzed by a monochromator (Jobin, Yvon Micro HR) and detected with a back-illuminated CCD (Syncerity S10420). Spectra were simulated by a linear combination of lognormal curves with a MATLAB script (least square fit). With the same set-up for excitation, the detection of fluorescence decay was measured by the way of a filter wheel and a Photomultiplier device (Hamamatsu H9305-01). The electric signal was recorded with an oscilloscope after pre-amplification (200 mHz of bandwidth). This detection

setup allows the detection of decay longer than 5 ns. After correction, decays were simulated by way of an exponential fit and a power-like law (MATLAB script).

2.3. Contact angle measurements

Static contact angles were measured on the untreated thin sections of the reservoir rock and of the non-reservoir rock. The measurements were performed with a Tracker Tensiometer from Teclis at room temperature. 2 μL-drops of standard brine of intermediate salinity (composition: NaCl = 32.3 g/L; $MgCl_2{\cdot}6H_2O$ = 12.6 g/L; $CaCl_2{\cdot}2H_2O$ = 1.7 g/L) were deposited on the samples using an automatic procedure. 12 and 7 drops were deposited in line for the non-reservoir rock and the reservoir rock respectively, to have statistical results. For all drops, the contact angle was measured after 120 s.

2.4. Atomic force microscopy and spectroscopy

The topographical features of the limestone sample were evaluated using Atomic Force Microscopy (AFM) operating in contact and dynamic mode [46]. All measurements were performed using a MFP-3D microscope from Asylum Research (Santa Barbara, USA) with a maximum travel of the piezo scanner of 120 μm in the planar direction (x,y) and 15 μm in the vertical direction (z). The microscope is isolated inside a chamber and further, it contains a vibration isolation control unit from Herzan. Complementary, the AFM contains an inverted optical microscope mounted on the AFM head that records optical images of the cantilever and the sample. All the AFM images were acquired by using triangular silicon nitride (PNP-TR from NanoWorld) with a nominal length of 200 μm, a width of 28 μm, and a thickness of 500 nm. The employed AFM probes had a nominal spring constant of 0.08 $N{\cdot}m^{-1}$ and were routinely calibrated using the thermal method. All the obtained images were processed using the AR and WSxM software [47].

Owing to the ability of thiols to form self-assembled monolayers (SAMs) on certain gold substrates, we functionalized gold-coated AFM tips (PNP-TR-Au from NanoWorld) with 35 nm of gold coating, according to supplier. The functionalization protocol starts with a UV/O_3 plasma treatment to clean gold coated-AFM tips for 20 min and after that, the tips are immersed into a 2 mM ethanolic solution of the desired thiol for at least 24 h. In this work, we have used undecanethiol and 11 mercaptoundecanoic acid to obtain hydrophobic and hydrophilic AFM tips, respectively. Functionalized tips are usually prepared before each experiment. Alternatively, the functionalized tips were stored in pure ethanol until they were used for force spectroscopy. The dimensions of either hydrophobic or hydrophilic monolayer resulted in an increase of about 2 nm in the tip radius. Before the experiment, the functionalized tip was dried by blowing Ar and then introduce into the AFM liquid cell where the thin section was immersed. After 30 min of system stabilization, AFS measurements were acquired in liquid medium at pH 6. Under these conditions, the carboxylate groups should be negatively charged and the measured forces would correspond to electrostatic forces rather than hydrogen bonding. We used these functionalized tips to measure adhesion force maps of 32 × 32 px (a pixel corresponds to the region where a force-distance curve is measured and from where adhesion force is determined), containing thus 1024 force-distance curves for each adhesion force map. We further covered different spatial scales (map size) from 60 μm to 1 μm which corresponds to acquisition of force-distance curves from every 2 μm to every 30 nm.

All the force spectroscopy measurements were performed in low salinity conditions (1 mM NaCl solution) using a loading force of 2 nN to avoid damage to the hydrocarbon monolayer. We also checked if we unintentionally modified the rock surface by depositing the organic monolayer of the functionalized tip during the AFS measurements across the scales which were performed keeping the same center and just reducing the image size. Thus, we routinely measured again the largest area (60 μm × 60 μm) and confirmed that neither the adhesion force nor the surface roughness of the carbonate surface was altered by the force spectroscopy measurements (Fig. S1).

3. Results and discussion

3.1. Does the scale of observation play a role in determining the wettability of carbonate rocks?

When studying the wettability properties of heterogeneous surfaces, such as carbonate rocks, the scale of observation can play an important role. At the macroscale, we measured the contact angle of our carbonate rocks (Fig. S2). For the non-reservoir and reservoir rocks, we obtained average values of 63.8 ± 3.4° and 73.4 ± 3.9° (mean ± SD) respectively, which indicates a mix-wet surface behavior for both although a more hydrophobic behavior was obtained for the reservoir rock. However, information about any potential heterogeneities is unavailable at this point. Observations of both limestone rocks using SEM and polarizing optical microscopy enabled the identification of the biologic constituents, as exemplified by the red algae fragment (ancient organism from eukaryotic algae presented as fossilized biomineral) of the non-reservoir rock sample (Fig. 2A–C). Such identification is fundamental for further measurements of the wettability properties of individual components of the carbonate rock from the micro- to the nano-scale.

To study the molecular interactions at the rock-water interface, we performed AFS experiments on the limestone surfaces over a spatial range from 60 μm down to 1 μm, thus measuring force-distance curves from every 2 μm to every 30 nm. Making use of an optical microscope integrated into the AFM unit, we intentionally placed the tip in the region of interest for the wettability measurements (Fig. 2C) and imaged the carbonate surface at different scales (Fig. 2D,E). We used CH_3-functionalized tips to directly probe hydrophobic interactions by simultaneously measuring the surface topography and adhesion force of the surface of carbonate bioclasts (see red algae in Fig. 2F,G and another examples Fig. S3). From the height differences in topography maps (Fig. 2F and Fig. S4), we determined the surface roughness of the rock by RMS (root mean square) method, which decreased across the scales. We found different topographic features with height variations from a few tens of nm to about 1 μm. On the one hand, images larger than 20 μm show the assemblage of mineral grains giving rise to specific textures of each type of bioclast that facilitate their recognition (see characteristic stripes of red algae and its height profile in Fig. S4A). On the other hand, for images smaller than 5 μm-size, the topography corresponds to clusters of nanometer-sized mineral grains with RMS < 200 nm (see Fig. S4B). Regarding the adhesion force maps, we observed minor differences in the mean adhesion values across the spatial scales studied, that is, image sizes in the range from 60 to 1 μm (Fig. S4C). Although the influence of surface roughness on the macroscopic wettability properties has been reported previously [48,49], we did not observe such a roughness effect on the mean adhesion data in the studied spatial resolution (Fig. S5). This suggests that nano-wettability is rather influenced by differences in the chemical composition of the rock surface than by differences in surface roughness. It is important to note that adhesion force values are highly dependent on the tip-surface contact area, which is very small and independent of the map size, resulting in similar

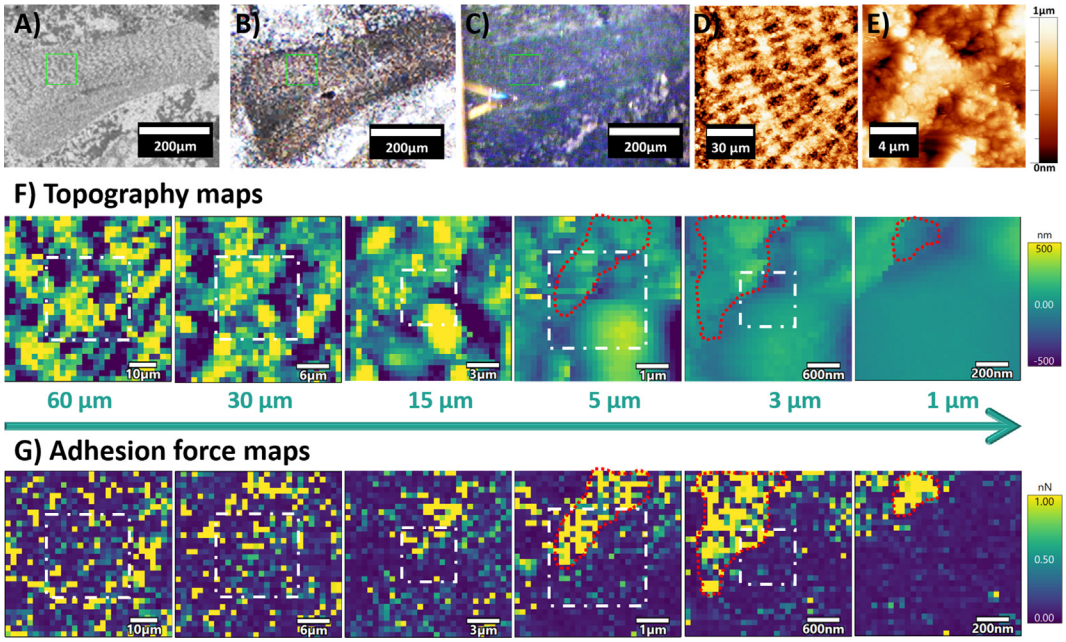

Fig. 2. Images of a bioclast of the non-reservoir rock that contains a red algae fragment obtained by: (A) SEM, (B) PPL optical microscope and (C) inverse optical microscope coupled with AFM microscope and where the AFM tip is also presented. (D,E) AFM images of the red algae area highlighted with a green square in images A-C at 120 and 20 µm image size. (F) Topography and (G) adhesion force maps obtained with a hydrophobic tip in a range of image sizes from 60 to 1 µm (white squares indicate where the next map of lower dimensions was acquired). Only below an image size of 5 µm, we observe homogeneous hydrophobic regions (highlighted with a contoured dotted line in red).

mean adhesion values. However, in the adhesion maps of Fig. 2G, we observed homogeneous hydrophobic regions only below 5 µm map size that are highlighted with a contoured red dotted line in Fig. 2G. This result demonstrates that the spatial distribution of the adhesion data does indeed allow us to identify homogeneous regions of high adhesion. Overall, these results confirm that the scale of observation is an important parameter when studying rock surface wettability.

3.2. Does adsorbed organic matter play a role in the wettability of carbonate rocks?

Once the relevant scale of observation is identified, the nano-wettability of the limestone rocks was explored using image sizes of 5 µm (where we observed homogeneous hydrophobic regions) and acquiring force maps with a resolution of 150 nm/px. The adhesion properties of the non-reservoir (Fig. 3A) and reservoir (Fig. 3B) rock samples were studied using CH_3- and COOH-functionalized tips as non-polar and polar probes to mimic hydrophobic and hydrophilic organic-carbonate interactions, respectively. Representative adhesion force maps obtained with the CH_3-tip (Fig. 3C,D) show higher adhesive-type interactions than those obtained with COOH-tip (Fig. 3E,F). The hydrophobic interactions are especially pronounced in the reservoir rock as evidenced by the larger adhesion force data (1.73 ± 0.29 nN) found in comparison to that of the non-reservoir rock (0.68 ± 0.09 nN). In addition to the preferential interaction of the reservoir rock surface with non-polar molecules, this rock type presents a highly homogeneous surface in terms of wetting behavior. In contrast, the non-reservoir rock presents distinct homogeneous sizes of hydrophobic and hydrophilic properties. Furthermore, our measurements with COOH-tips led to slightly higher adhesion force in the non-reservoir rock (0.74 ± 0.1 nN) than in the reservoir rock (0.68 ± 0.09 nN). Looking at representative force-distance curves of both carbonate rocks using CH_3- and COOH-tips (Fig. S6), we observed that the approaching curves usually present a slight electrostatic repulsion with the exception when the CH_3-tip approaches to the reservoir rock surface, which presents an attractive force at a separation distance of 15 nm (hydrophobic or Van der Waals interactions). According to the DLVO theory, a low electric double layer (EDL) repulsion was expected between rock surface with little or no charge and the low salinity conditions of the solution (low ionic strength). However, the strong attractive interaction between the hydrophobic tip and the reservoir rock surface is evidence of the higher hydrophobicity of this rock. The adhesion peaks in the retracting curves correspond to the hydrophobic or hydrophilic interactions depending on the use of CH_3- or COOH-tips, respectively. The reservoir rock surface presents the largest adhesion peak when interacting with the CH_3-tip (7.4 nN), whereas a very small adhesion peak is observed when using COOH-tip (0.1 nN), confirming its predominant hydrophobic character due to the high amount of organic material. However, similar (low) adhesion peaks are observed in the interactions of the hydrophobic and hydrophilic tips with the non-reservoir rock (1.2 and 0.7 nN, respectively), ascribed to a lower content of organic matter.

Statistical analysis of our AFS results (about 250.000 force-distance curves for both rocks and both functionalized tips) was done to obtain representative wettability data of the rock surface from nanoscale interactions. The statistical results are presented as adhesion histograms in Fig. 3G,H and confirm the stronger hydrophobic behavior of the reservoir rock in comparison with that of the non-reservoir rock. In agreement with the macroscopic contact angle measurements (Fig. S2), these nanoscale measurements reveal the critical role that foreign organic matter (i.e. oil) plays in controlling the surface wettability.

3.3. Is the wettability linked to the biogenicity of a rock fragment?

Hydrophobic interactions of both carbonate rocks were further explored and related to their biological origin, classifying them into different types of bioclasts. Before AFS measurements (Fig. 4A), the

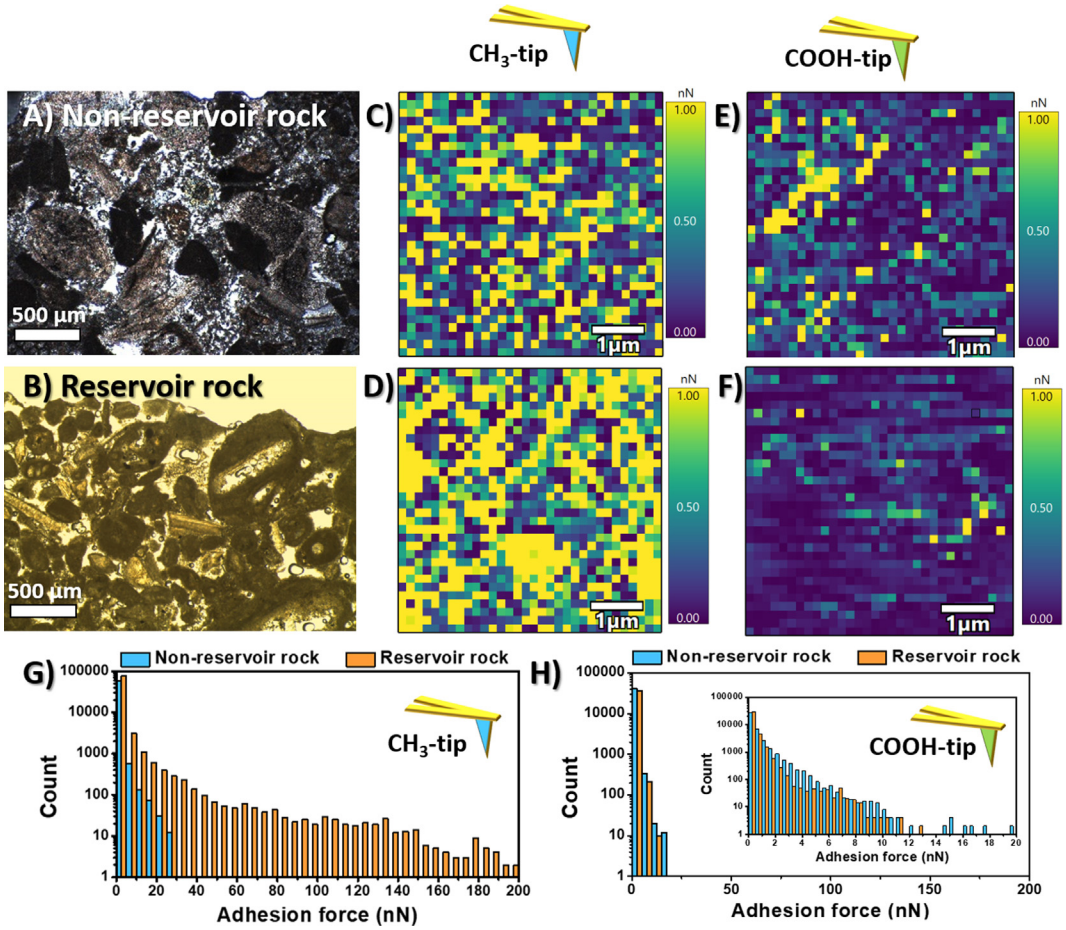

Fig. 3. Thin section optical images of (A) non-reservoir and (B) reservoir carbonate rocks where AFS measurements were performed. Representative adhesion force maps were obtained in both rocks using the hydrophobic (C,D) and hydrophilic (E,F) tips. Adhesion force histograms corresponding to 75,000 force-curve data (G) CH_3-tip and H) COOH-tip.

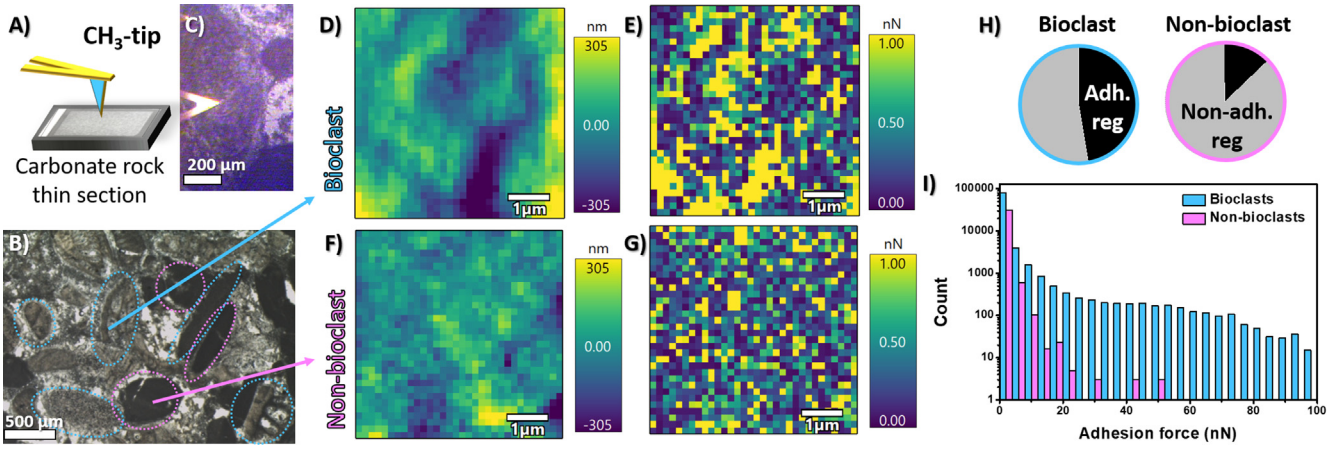

Fig. 4. (A) Schematic representation of the AFS measurements using CH_3-tips and carbonate thin sections. (B) Optical micrograph of the non-reservoir carbonate rock thin section. (D) Topography and (E) adhesion force maps of bioclasts in comparison with (F) topography and (G) adhesion force maps of non-bioclasts. (H) Pie-chart representing the percentage of adhesion region measured over the total map area for bioclasts and non-bioclasts. (I) Adhesion force histograms of the AFS measurements.

carbonate thin sections were observed with a polarizing optical microscope to identify the components of the rocks (Fig. 4B). We classified the rock components as bioclasts or skeletal grains with biological origin and non-bioclast including non-skeletal grains and types of cement. Then, we explored if the bioclasts influence the rock wettability of the non-reservoir and reservoir rocks using AFM and an integrated optical microscope (Fig. 4C). Although trivial, the identification of rock constituents from the micro- to the nano-scale has been fundamental to understand the wettability properties of the rocks. The topography and adhesion force maps of Fig. 4D–G show larger hydrophobic regions in the bioclast regions (Fig. 4D–E) than in the non-bioclasts ones (Fig. 4F–G). In

fact, we calculated from multiple force maps that the adhesive region in bioclasts corresponds to 47 % of the imaged area, while for non-bioclasts it only represents 13 % (Fig. 4H). Furthermore, adhesion histograms, corresponding to the analysis of 150.000 force-distance curves (Fig. 4I), confirm that bioclast regions interact more strongly with the hydrophobic tip than the non-bioclast ones. However, we did not observe any relevant inter-biomineral differences, i.e. echinoderm, mollusk, foraminifera, bryozoan and red algae all displayed comparable values of adhesion (Fig. S7). We have used the non-parametric test Krusal-Wallis test to find out whether there are significant differences between the adhesion force data shown in the histograms of Fig. 4. The results of this statistical test reveal a significant difference between the two sets of samples at the 95 % confidence level (p values < 2.2e−16, chi-squared = 194.69).The significant difference in the wettability (Fig. S8) between bioclasts (0.80 and 2.89 nN for non-reservoir and reservoir rock) and non-bioclasts (0.56 and 1.35 nN for non-reservoir and reservoir rock) can be ascribed to the presence of organic remains within the former (indeed, biominerals are composite organo-mineral materials). The organic remainders favor interactions with non-polar organic molecules. Fossilized biominerals can therefore induce hydrophobicity, also facilitating the adsorption of organic matter (i.e. in oil reservoirs) through non-polar interactions.

3.4. Evaluating the role of organic matter on the wettability properties of carbonate rocks

Based on our nanoscale observations, we have established that a more hydrophobic behavior is present in the reservoir rock. Furthermore, we have observed a significant difference between the wetting properties of bioclast and non-bioclast grains. These results highlight the key role that organic matter, either adsorbed hydrocarbons from crude oil or gas or the breakdown products of biomolecules included in biominerals, plays on the wettability (hydrophobicity) of rock surfaces. To identify the presence of organic matter in the carbonate rock surface, we performed Raman microspectroscopy on thin sections of both limestone rocks. In addition to the calcite peaks in the low wavenumber region (calcite is the dominant calcium carbonate polymorph (Fig. S9), we also detected the fingerprints of organic matter in the higher wavenumber region (Fig. 5A). In particular, we observed the characteristic D and G bands of graphitic structures, which are attributed to in-plane defects and sp^2 C—C stretching vibrations within the aromatic rings of the graphitic layer, respectively [50]. The presence of wide D and G bands with similar intensities indicates the presence of disordered organic matter in all the samples. However, their distribution on the surface differs: the bioclasts, non-bioclasts and cement components of the reservoir rock present a homogeneous distribution on the rock surface (Fig. S10). But, for the non-reservoir rock, the signal from organic matter was only presented in the bioclastic grains. These results support the idea that the presence of organic matter from a natural origin is responsible for the hydrophobic behavior. Also, these maps with a resolution of 1 μm/px agree well with the spatial heterogeneity observed in the wetting properties at small spatial scales.

The position and broadening of D and G bands were determined by simultaneous peak fitting to Lorentzian profiles after baseline correction to remove the fluorescence contribution of the organic matter using Quasar software [45]. (Fig. 5B). Based on the Raman observations in the bioclasts of the non-reservoir rock (Fig. 5C), the position of the G band at 1580 cm^{-1} corresponds to that of crystalline graphitic structure and the D band at 1347 cm^{-1} of high intensity indicates the presence of heteroatoms such as hydrogen, nitrogen or oxygen in the aromatic rings of the organic matter [51]. For the reservoir rock, we observed a significant blue-shift in the D and the G bands, being larger for the bioclasts (1375 and 1595 cm^{-1}) than for the non-bioclasts, including grains and cements (1370 and 1591 cm^{-1}). The shift in the G peak has been attributed to the presence of hydrocarbons adsorbed on the rock surface from the crude oil [52]. The G peaks of the bioclasts are also narrower than those of the non-bioclast grains and cements (Fig. S11), which reveals a higher degree of graphitization of the organic molecules in the bioclast grains. This effect is also reflected in the shift of the D peak of the reservoir rock, which has been previously attributed to a higher degree of maturation of the organic matter in rocks [53].

Additionally, we explored the fluorescence of organic matter contained in our carbonate rocks in the wavelength range of 300–800 nm using an excitation wavelength of 266 nm. We explored a large area of 18 mm^2 on thin sections of both carbonate rocks to observe the emission of the different components. Fluorescence intensity maps at 340 nm (Fig. 6A) and 420 nm (Fig. 6B) of non-reservoir and reservoir rocks reveal that the former contribution is characteristic of the bioclast grains. Here, the spatial resolution of the fluorescence maps does not allow for the observation of heterogeneities in the nanoscale but still gives relevant insights into the composition of the organic matter of the carbonate rocks. Fig. 6C shows representative spectra of bioclast and non-bioclast grains in both rocks and their fits. The fit results clearly show the presence of the peak around 340 nm (purple line) in the bioclasts – especially that of the reservoir rock – whereas it is negligible for the non-bioclasts. The fluorescence around 420 nm (blue line) is the main component of all the rock constituents. This peak is considerably wider in the bioclasts, attributed to the presence of multiple fluorophores although less intense than in the non-bioclasts. Finally, we observed a third contribution (magenta line) with an emission center around 500 nm in the bioclasts and shifted to 450 nm in the case of the non-bioclasts grains.

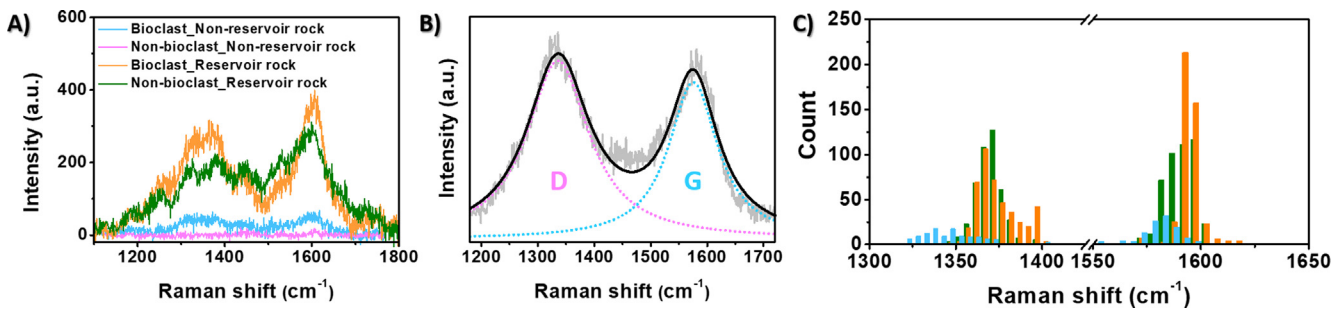

Fig. 5. (A) Raman spectra of C-signal region for the bioclasts and non-bioclasts of (including grains and cements) non-reservoir and reservoir rocks. (B) Example of a double Lorentzian fit ascribed to the D (pink) and G (blue) bands of graphitic structures. (C) Distributions of D and G band position obtained from Raman mapping of 10 × 10 μm × μm spatial areas with a resolution of 0.5 μm for the bioclasts of the non-reservoir rock (blue) and the bioclasts (orange) and non-bioclasts (green) of the reservoir rock.

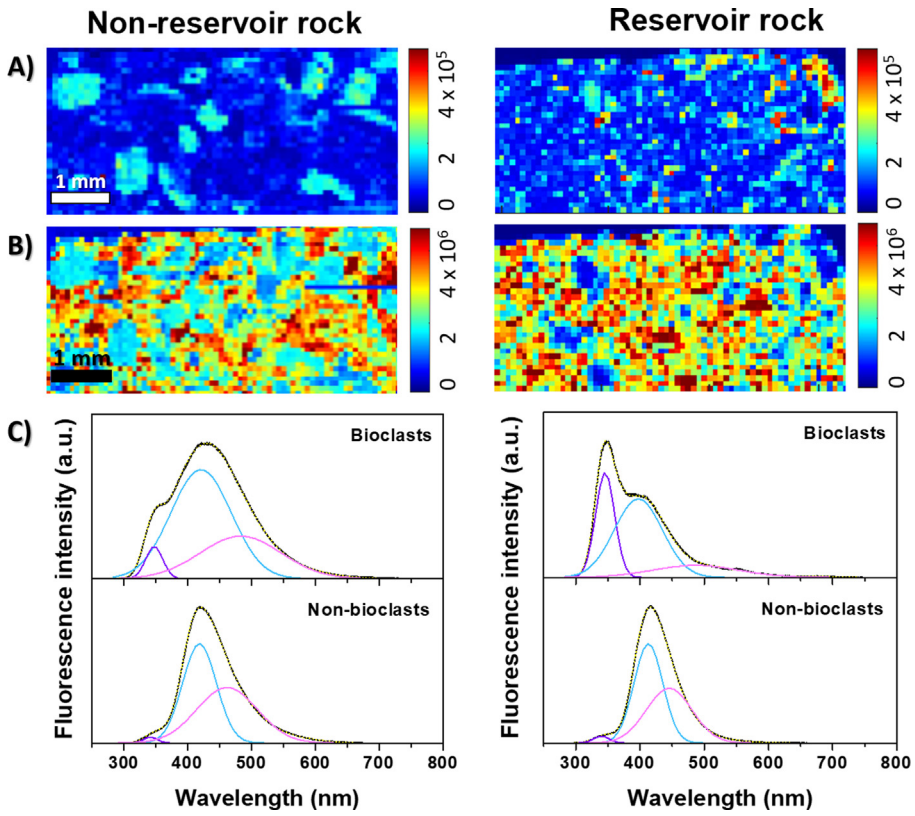

Fig. 6. Stationary fluorescence intensity maps for wavelengths of (A) 340 and (B) 450 nm for non-reservoir (left) and reservoir rocks (right) with a resolution of 100 μm. (C) Representative fluorescence spectra of bioclasts and non-bioclasts for non-reservoir (left) and reservoir rocks (right) together to their fit using 3 gaussian peaks around 340 (purple), 420 (blue) and 500 nm (magenta).

We have further measured decay spectra in the bioclasts and non-bioclast grains of both rocks for the three contributions observed in the stationary fluorescence. The decay times were simulated with Power-like function estimations [54] for each of the center wavelengths using and passband filter with 10 nm wavelength width. For the 340 and the 420 nm bands, decay times are low and close to the detection limit of our setup, typically between 5 and 6 ns. These results suggest that the fluorescence at 340 and 420 nm could correspond to small organic molecules rather than polyaromatic molecules which are known to exhibit a long-time decay fluorescence [55,56]. The 500 nm centered band shows a longer fluorescence decay time on the bioclast, longer than 8 ns whereas, for non-bioclast, fluorescence decay time remains between 5 and 6 ns. Furthermore, we observed a high sensitivity of the contribution around 340 and 420 nm to photodegradation (Fig. S12) whereas the contribution around 500 nm remains constant. This result together with the longer time decay on bioclast indicates that some biological compounds such as protein-like or humic-like (also referred to as unidentified natural organic compounds – UNOC) are present in the carbonate rocks and partially trapped by the bioclasts [57,58]. Overall, we found that bioclasts show a different fluorescence spectrum than that of the non-bioclasts with a contribution around 340 nm that furthermore, becomes the main component in the reservoir rock. Since these results are highly in concordance with the wettability of the bioclasts, we ascribe the emission at 340 nm to organic matter of organic behavior with a plausible biological origin.

4. Conclusion

There is a common use to describe the wettability of a surface sample by using contact angle measurements [59]. However, the macro-scale approach of such measurements only provides an average bulk value of the solid surface, missing thus valuable information from the nanoscale. In this sense, AFM has appeared as a good alternative to explore the mineral/liquid interface and determine the surface nano-wettability of various minerals as well as the effect of fluid composition [25–29]. Our AFM/AFS approach probing molecular interactions within carbonate rocks allows elucidating the complexity of rock surface wettability, especially in heterogeneous natural systems, by exploring surface heterogeneities from the micro- to the nano-scale. We demonstrate that the scale of observation is an important parameter when describing the wettability properties of natural rocks, being necessary to explore areas below 25 μm^2 to study heterogeneities of the carbonate rock. At this length scale, preferential interaction (stronger adhesion force) with hydrophobic molecules showed a homogeneous wetting behavior of the reservoir rock. However, at the same length scale, the non-reservoir rock presented heterogeneous hydrophobic regions only at the surface of biominerals. This result is in line with the literature reporting heterogeneities in the carbonate rock wettability as a consequence of the presence of organic matter [24,34,35] and could be complemented using other hydrophilic functionalization (NH_2- and OH-tips) or partial hydrophilic functionalization (OCH_3-tips).

Furthermore, our methodology with the identification of individual components of the carbonate rock from the micro- to the nano-scale represents a new innovative approach that has been fundamental in exploring the wettability of specific bioclast and non-bioclast grains, resulting that the former presents higher hydrophobic behavior. The combination of adhesion force maps with micro-Raman and especially with fluorescence spectroscopy maps has resulted in a success for detecting organic matter and determining the type and abundance of organic molecules on

mineral surfaces. Thus, the spectroscopy results have confirmed the hypothesis that organic remains within the biominerals is primarily responsible for the hydrophobic character of bioclast grain surfaces. The fluorescence emission of the carbonate rocks confirmed the presence of organic matter which experiments photobleaching at long time exposition. The main signals correspond to protein-like or humic-like compounds and their short decay times reveal that small molecules with certain aromaticity are present in the rock. A high degree of maturation, observed in the position of the C signal in the Raman spectra, elucidates that small molecules with natural origin (i.e. amino acids) can be present within the rock which leads to homogeneous hydrophobic regions. Future synchrotron experiments would shed light on the composition of the organic matter present in the specific grains of these limestones and establish a direct relation with its wettability properties.

Overall, this work contributes to the understanding of surface wettability properties of carbonate rocks by establishing the spatial scale necessary to study heterogeneities in wettability, which can potentially control the overall wettability of the rock. All results together (Table S3) highlight the critical role that the biogenic origin of the minerals plays in the wetting behavior of the limestones at the nanoscale, which had never been studied up to now. Furthermore, we propose that the rock composition in terms of bioclastic content could be used as a potential parameter to control the wettability properties of carbonate-water interfaces. This could have a direct impact on various geological, environmental, and industrial processes where solid–liquid interfaces play a key role in the overall efficiency of processes such as CO_2 sequestration or enhanced oil recovery techniques [60,61].

CRediT authorship contribution statement

Alicia Moya: Investigation, Data curation, Visualization, Formal analysis, Methodology, Validation, Writing – original draft, Writing – review & editing. **Fabienne Giraud:** Investigation, Validation, Writing – review & editing. **Valerie Molinier:** Investigation, Resources, Writing – review & editing. **Yves Perrette:** Investigation, Data curation, Formal analysis, Methodology, Writing – review & editing. **Laurent Charlet:** Conceptualization, Resources, Supervision, Funding acquisition, Writing – review & editing. **Alexander Van Driessche:** Conceptualization, Resources, Supervision, Funding acquisition, Writing – review & editing. **Alejandro Fernandez-Martinez:** Conceptualization, Resources, Supervision, Funding acquisition, Writing – review & editing.

Data availability

The data that support the plots within this paper and other findings of this study are available from the corresponding author upon reasonable request.

Declaration of Competing Interest

The authors declare that they have no known competing financial interests or personal relationships that could have appeared to influence the work reported in this paper.

Acknowledgments

We thank Ms. Laura Pauliet for performing the contact angle measurements in TotalEnergies laboratories and Mr. Sylvan Campillo for ICP measurements in ISTerre. We acknowledge funding from Labex OSUG@2020 Equipment.

Appendix A. Supplementary material

Supplementary data to this article can be found online at https://doi.org/10.1016/j.jcis.2023.03.197.

References

[1] J.W.N. Smith, D.N. Lerner, Geomorphologic control on pollutant retardation at the groundwater–surface water interface, Hydrol. Process. 22 (2008) 4679–4694, https://doi.org/10.1002/hyp.7078.
[2] B. Ma, L. Charlet, A. Fernandez-Martinez, M. Kang, B. Madé, A review of the retention mechanisms of redox-sensitive radionuclides in multi-barrier systems, Appl. Geochem. 100 (2019) 414–431, https://doi.org/10.1016/j.apgeochem.2018.12.001.
[3] S. Elhadj, J.J.D. Yoreo, J.R. Hoyer, P.M. Dove, Role of molecular charge and hydrophilicity in regulating the kinetics of crystal growth, Proc. Natl. Acad. Sci. 103 (2006) 19237–19242, https://doi.org/10.1073/pnas.0605748103.
[4] E.M. Dettenmaier, W.J. Doucette, B. Bugbee, Chemical hydrophobicity and uptake by plant roots, Environ. Sci. Tech. 43 (2009) 324–329, https://doi.org/10.1021/es801751x.
[5] U. Hübner, C. Wurzbacher, D.E. Helbling, J.E. Drewes, Engineering of managed aquifer recharge systems to optimize biotransformation of trace organic chemicals, Curr. Opin. Environ. Sci. Health. 27 (2022), https://doi.org/10.1016/j.coesh.2022.100343 100343.
[6] C.J. Bronick, R. Lal, Soil structure and management: a review, Geoderma 124 (2005) 3–22, https://doi.org/10.1016/j.geoderma.2004.03.005.
[7] A. Raza, R. Gholami, M. Sarmadivaleh, Feasibility of limestone reservoirs as a carbon dioxide storage site: an experimental study, AAPG Bull. 104 (2020) 83–96, https://doi.org/10.1306/04241918124.
[8] A. Gandomkar, M.R. Rahimpour, Investigation of low-salinity waterflooding in secondary and tertiary enhanced oil recovery in limestone reservoirs, Energy Fuels 29 (2015) 7781–7792, https://doi.org/10.1021/acs.energyfuels.5b01236.
[9] R. Anderson, L. Zhang, Y. Ding, M. Blanco, X. Bi, D.P. Wilkinson, A critical review of two-phase flow in gas flow channels of proton exchange membrane fuel cells, J. Power Sources 195 (2010) 4531–4553, https://doi.org/10.1016/j.jpowsour.2009.12.123.
[10] O. Lehmann, L. Birnhack, O. Lahav, Design aspects of calcite-dissolution reactors applied for post treatment of desalinated water, Desalination 314 (2013) 1–9, https://doi.org/10.1016/j.desal.2012.12.017.
[11] D. Hasson, L. Fine, A. Sagiv, R. Semiat, H. Shemer, Modeling remineralization of desalinated water by micronized calcite dissolution, Environ. Sci. Tech. 51 (2017) 12481–12488, https://doi.org/10.1021/acs.est.7b03069.
[12] M. Lim, G.-C. Han, J.-W. Ahn, K.-S. You, Environmental remediation and conversion of carbon dioxide (CO2) into useful green products by accelerated carbonation technology, Int. J. Environ. Res. Public Health 7 (2010), https://doi.org/10.3390/ijerph7010203.
[13] E.C. Donaldson, W. Alam, CHAPTER 1 - Wettability, in: E.C. Donaldson, W. Alam (Eds.), Wettability, Gulf Publishing Company, 2008, pp. 1–55, doi: 10.1016/B978-1-933762-29-6.50007-7.
[14] I. Gupta, J. Jernigen, M. Curtis, C. Rai, C. Sondergeld, Water-wet or oil-wet: is it really that simple in shales? Petrophysics - SPWLA, J. Form. Eval. Reserv. Descr. 59 (2018) 308–317. 10.30632/PJV59N3-2018a2.
[15] H.J. Deglint, C.R. Clarkson, C. DeBuhr, A. Ghanizadeh, Live imaging of micro-wettability experiments performed for low-permeability oil reservoirs, Sci. Rep. 7 (2017) 4347, https://doi.org/10.1038/s41598-017-04239-x.
[16] A. Ivanova, N. Mitiurev, A. Cheremisin, A. Orekhov, R. Kamyshinsky, A. Vasiliev, Characterization of organic layer in oil carbonate reservoir rocks and its effect on microscale wetting properties, Sci. Rep. 9 (2019) 10667, https://doi.org/10.1038/s41598-019-47139-y.
[17] M.A.Q. Siddiqui, S. Ali, H. Fei, H. Roshan, Current understanding of shale wettability: a review on contact angle measurements, Earth Sci. Rev. 181 (2018) 1–11, https://doi.org/10.1016/j.earscirev.2018.04.002.
[18] M. Seyyedi, M. Sohrabi, A. Farzaneh, Investigation of rock wettability alteration by carbonated water through contact angle measurements, Energy Fuels 29 (2015) 5544–5553, https://doi.org/10.1021/acs.energyfuels.5b01069.
[19] W. Abdallah, A. Gmira, Wettability assessment and surface compositional analysis of aged calcite treated with dynamic water, Energy Fuels 28 (2014) 1652–1663, https://doi.org/10.1021/ef401908w.
[20] K. Huang, P. Rowe, C. Chi, V. Sreepal, T. Bohn, K.-G. Zhou, Y. Su, E. Prestat, P.B. Pillai, C.T. Cherian, A. Michaelides, R.R. Nair, Cation-controlled wetting properties of vermiculite membranes and its promise for fouling resistant oil–water separation, Nat. Commun. 11 (2020) 1097, https://doi.org/10.1038/s41467-020-14854-4.
[21] R. Barattin, N. Voyer, Chemical modifications of AFM tips for the study of molecular recognition events, Chem. Commun. (2008) 1513–1532, https://doi.org/10.1039/B614328H.
[22] Y. Xia, Y. Xing, M. Li, M. Liu, J. Tan, Y. Cao, X. Gui, Studying interactions between undecane and graphite surfaces by chemical force microscopy and molecular dynamics simulations, Fuel 269 (2020), https://doi.org/10.1016/j.fuel.2020.117367 117367.
[23] W. Zhang, H. Yang, F. Liu, T. Chen, G. Hu, D. Guo, Q. Hou, X. Wu, Y. Su, J. Wang, Molecular interactions between DOPA and surfaces with different functional groups: a chemical force microscopy study, RSC Adv. 7 (2017) 32518–32527, https://doi.org/10.1039/C7RA04228K.

[24] T. Hassenkam, L.L. Skovbjerg, S.L.S. Stipp, Probing the intrinsically oil-wet surfaces of pores in North Sea chalk at subpore resolution, Proc. Natl. Acad. Sci. 106 (2009) 6071–6076, https://doi.org/10.1073/pnas.0901051106.
[25] D. Afekare, J.C. Garno, D. Rao, Insights into nanoscale wettability effects of low salinity and nanofluid enhanced oil recovery techniques, Energies 13 (2020), https://doi.org/10.3390/en13174443.
[26] J. Wu, F. Liu, H. Yang, S. Xu, Q. Xie, M. Zhang, T. Chen, G. Hu, J. Wang, Effect of specific functional groups on oil adhesion from mica substrate: implications for low salinity effect, J. Ind. Eng. Chem. 56 (2017) 342–349, https://doi.org/10.1016/j.jiec.2017.07.030.
[27] S. Yesufu-Rufai, M. Rücker, S. Berg, S.F. Lowe, F. Marcelis, A. Georgiadis, P. Luckham, Assessing the wetting state of minerals in complex sandstone rock in-situ by Atomic Force Microscopy (AFM), Fuel 273 (2020), https://doi.org/10.1016/j.fuel.2020.117807 117807.
[28] S. Yesufu-Rufai, F. Marcelis, A. Georgiadis, S. Berg, M. Rücker, J. van Wunnik, P. Luckham, Atomic Force Microscopy (AFM) study of redox conditions in sandstones: Impact on wettability modification and mineral morphology, Colloids Surf. Physicochem. Eng. Asp. 597 (2020), https://doi.org/10.1016/j.colsurfa.2020.124765 124765.
[29] T. Hassenkam, C.S. Pedersen, K. Dalby, T. Austad, S.L.S. Stipp, Pore scale observation of low salinity effects on outcrop and oil reservoir sandstone, Colloids Surf. Physicochem. Eng. Asp. 390 (2011) 179–188, https://doi.org/10.1016/j.colsurfa.2011.09.025.
[30] J. Matthiesen, N. Bovet, E. Hilner, M.P. Andersson, D.A. Schmidt, K.J. Webb, K.N. Dalby, T. Hassenkam, J. Crouch, I.R. Collins, S.L.S. Stipp, How naturally adsorbed material on minerals affects low salinity enhanced oil recovery, Energy Fuels 28 (2014) 4849–4858, https://doi.org/10.1021/ef500218x.
[31] E. Hilner, M.P. Andersson, T. Hassenkam, J. Matthiesen, P.A. Salino, S.L.S. Stipp, The effect of ionic strength on oil adhesion in sandstone – the search for the low salinity mechanism, Sci. Rep. 5 (2015) 9933, https://doi.org/10.1038/srep09933.
[32] B. Lorenz, M. Ceccato, M.P. Andersson, S. Dobberschütz, J.D. Rodriguez-Blanco, K.N. Dalby, T. Hassenkam, S.L.S. Stipp, Salinity-dependent adhesion response properties of aluminosilicate (K-feldspar) surfaces, Energy Fuels 31 (2017) 4670–4680, https://doi.org/10.1021/acs.energyfuels.6b02969.
[33] N.R. Pedersen, T. Hassenkam, M. Ceccato, K.N. Dalby, K. Mogensen, S.L.S. Stipp, Low salinity effect at pore scale: probing wettability changes in middle east limestone, Energy Fuels 30 (2016) 3768–3775, https://doi.org/10.1021/acs.energyfuels.5b02562.
[34] J. Generosi, M. Ceccato, M.P. Andersson, T. Hassenkam, S. Dobberschütz, N. Bovet, S.L.S. Stipp, Calcite wettability in the presence of dissolved Mg2+ and SO42–, Energy Fuels 31 (2017) 1005–1014, https://doi.org/10.1021/acs.energyfuels.6b02029.
[35] J. Matthiesen, T. Hassenkam, N. Bovet, K.N. Dalby, S.L.S. Stipp, Adsorbed organic material and its control on wettability, Energy Fuels 31 (2017) 55–64, https://doi.org/10.1021/acs.energyfuels.6b00627.
[36] S. Mann, Molecular recognition in biomineralization, Nature 332 (1988) 119–124, https://doi.org/10.1038/332119a0.
[37] M.P. Andersson, K. Dideriksen, H. Sakuma, S.L.S. Stipp, Modelling how incorporation of divalent cations affects calcite wettability–implications for biomineralisation and oil recovery, Sci. Rep. 6 (2016) 28854, https://doi.org/10.1038/srep28854.
[38] M. Shakeel, P. Pourafshary, M. Rehan Hashmet, Hybrid engineered water-polymer flooding in carbonates: a review of mechanisms and case studies, Appl. Sci. 10 (2020), https://doi.org/10.3390/app10176087.
[39] M. Dernaika, M. Al Mansoori, M. Singh, T. Al Dayyani, Z. Kalam, R. Bhakta, S. Koronfol, Y.N. Uddin, Digital and conventional techniques to study permeability heterogeneity in complex carbonate rocks, petrophysics - SPWLA J. Form, Eval. Reserv. Descr. 59 (2018) 373–396. 10.30632/PJV59N3-2018a6.
[40] A. Hosa, R. Wood, Order of diagenetic events controls evolution of porosity and permeability in carbonates, Sedimentology 67 (2020) 3042–3054, https://doi.org/10.1111/sed.12733.
[41] W.J. Kennedy, Trace fossils in carbonate rocks, in: R.W. Frey (Ed.), Study Trace Foss. Synth. Princ. Probl. Proced. Ichnology, Springer Berlin Heidelberg, Berlin, Heidelberg, 1975, pp. 377–398, https://doi.org/10.1007/978-3-642-65923-2_17.
[42] A.M.J. Fichtinger-Schepman, J.P. Kamerling, J.F.G. Vliegenthart, E.W. De Jong, L. Bosch, P. Westbroek, Composition of a methylated, acidic polysaccharide associated with coccoliths of *Emiliania huxleyi* (Lohmann) Kamptner, Carbohydr. Res. 69 (1979) 181–189, https://doi.org/10.1016/S0008-6215(00)85763-8.
[43] D.V. Zamarreño, R. Inkpen, M. Eric, Carbonate crystals precipitated by freshwater bacteria and their use as a limestone consolidant, Appl. Environ. Microbiol. 75 (2009) 5981–5990, https://doi.org/10.1128/AEM.02079-08.
[44] Y.-Y. Kim, K. Ganesan, P. Yang, A.N. Kulak, S. Borukhin, S. Pechook, L. Ribeiro, R. Kröger, S.J. Eichhorn, S.P. Armes, B. Pokroy, F.C. Meldrum, An artificial biomineral formed by incorporation of copolymer micelles in calcite crystals, Nat. Mater. 10 (2011) 890–896, https://doi.org/10.1038/nmat3103.
[45] M. Toplak, G. Birarda, S. Read, C. Sandt, S.M. Rosendahl, L. Vaccari, J. Demšar, F. Borondics, Infrared orange: connecting hyperspectral data with machine learning, Synchrotron Radiat. News. 30 (2017) 40–45, https://doi.org/10.1080/08940886.2017.1338424.
[46] P.J. de Pablo, J. Colchero, M. Luna, J. Gómez-Herrero, A.M. Baró, Tip-sample interaction in tapping-mode scanning force microscopy, Phys. Rev. B 61 (2000) 14179–14183, https://doi.org/10.1103/PhysRevB.61.14179.
[47] I. Horcas, R. Fernández, J.M. Gómez-Rodríguez, J. Colchero, J. Gómez-Herrero, A.M. Baro, WSXM: a software for scanning probe microscopy and a tool for nanotechnology, Rev. Sci. Instrum. 78 (2007), https://doi.org/10.1063/1.2432410 013705.
[48] A.M. Alhammadi, A. AlRatrout, K. Singh, B. Bijeljic, M.J. Blunt, In situ characterization of mixed-wettability in a reservoir rock at subsurface conditions, Sci. Rep. 7 (2017) 10753, https://doi.org/10.1038/s41598-017-10992-w.
[49] X. Wang, Q. Zhang, Insight into the influence of surface roughness on the wettability of apatite and dolomite, Minerals 10 (2020), https://doi.org/10.3390/min10020114.
[50] M.A. Pimenta, G. Dresselhaus, M.S. Dresselhaus, L.G. Cançado, A. Jorio, R. Saito, Studying disorder in graphite-based systems by Raman spectroscopy, PCCP 9 (2007) 1276–1290, https://doi.org/10.1039/B613962K.
[51] Y. Kebukawa, M.E. Zolensky, Q.H.S. Chan, K. Nagao, A.L.D. Kilcoyne, R.J. Bodnar, C. Farley, Z. Rahman, L. Le, G.D. Cody, Characterization of carbonaceous matter in xenolithic clasts from the Sharps (H3.4) meteorite: constraints on the origin and thermal processing, Geochim. Cosmochim. Acta 196 (2017) 74–101, https://doi.org/10.1016/j.gca.2016.09.024.
[52] J.S. Riedeman, N.R. Kadasala, A. Wei, H.I. Kenttämaa, Characterization of asphaltene deposits by using mass spectrometry and Raman spectroscopy, Energy Fuels 30 (2016) 805–809, https://doi.org/10.1021/acs.energyfuels.5b02002.
[53] Q.H.S. Chan, A. Stephant, I.A. Franchi, X. Zhao, R. Brunetto, Y. Kebukawa, T. Noguchi, D. Johnson, M.C. Price, K.H. Harriss, M.E. Zolensky, M.M. Grady, Organic matter and water from asteroid Itokawa, Sci. Rep. 11 (2021) 5125, https://doi.org/10.1038/s41598-021-84517-x.
[54] J. Włodarczyk, B. Kierdaszuk, Kinetics of triplet excitation transport in disordered organic solids, Chem. Phys. 297 (2004) 139–142, https://doi.org/10.1016/j.chemphys.2003.10.021.
[55] J. René Albani, Fluorescence lifetimes of tryptophan: structural origin and relation with So → 1Lb and So → 1La transitions, J. Fluoresc. 19 (2009) 1061, https://doi.org/10.1007/s10895-009-0506-7.
[56] M. Rasouli, S.H. Tavassoli, S.J. Mousavi, S.M.R. Darbani, Measuring of naphthalene fluorescence emission in the water with nanosecond time delay laser induced fluorescence spectroscopy method, Optik 127 (2016) 6218–6223, https://doi.org/10.1016/j.ijleo.2016.04.081.
[57] J.F. Power, R. LeSage, D.K. Sharma, C.H. Langford, Fluorescence lifetimes of the well characterized humic substance, armdale fulvic acid, Environ. Technol. Lett. 7 (1986) 425–430, https://doi.org/10.1080/09593338609384429.
[58] V. Bresler, V. Yanko, Chemical ecology; a new approach to the study of living benthic epiphytic foraminifera, J. Foramin. Res. 25 (1995) 267–279, https://doi.org/10.2113/gsjfr.25.3.267.
[59] S. Al-Anssari, A. Barifcani, S. Wang, L. Maxim, S. Iglauer, Wettability alteration of oil-wet carbonate by silica nanofluid, J. Colloid Interface Sci. 461 (2016) 435–442, https://doi.org/10.1016/j.jcis.2015.09.051.
[60] A.M. Selem, N. Agenet, M.J. Blunt, B. Bijeljic, Pore-scale processes in tertiary low salinity waterflooding in a carbonate rock: micro-dispersions, water film growth, and wettability change, J. Colloid Interface Sci. 628 (2022) 486–498, https://doi.org/10.1016/j.jcis.2022.06.063.
[61] J. Song, Q. Wang, I. Shaik, M. Puerto, P. Bikkina, C. Aichele, S.L. Biswal, G.J. Hirasaki, Effect of salinity, Mg2+ and SO42− on "smart water"-induced carbonate wettability alteration in a model oil system, J. Colloid Interface Sci. 563 (2020) 145–155, https://doi.org/10.1016/j.jcis.2019.12.040.